

# Fourier Transform Spectroscopy of Solids at Terahertz Frequencies

T J Parker

Physics Centre, University of Essex, Colchester, Essex CO4 3SQ, UK

E-mail: [etpkr@yahoo.co.uk](mailto:etpkr@yahoo.co.uk)

**Abstract:** We briefly review the techniques of dispersive Fourier transform spectroscopy (DFTS), polarised oblique incidence reflection spectroscopy and attenuated total reflection (ATR) spectroscopy, and discuss applications of these techniques to a variety of solids, including alkali halide crystals, pseudo-displacive ferroelectrics, and bulk and low-dimensional semiconductors.

**Keywords:** DFTS, ATR, polarised oblique incidence reflectivity, ionic solids, ferroelectrics, semiconductors

doi: 10.11906/TST.075-089.2009.09.09

## 1. DFTS techniques

Dispersive Fourier transform spectroscopy (DFTS) is an experimental technique which allows the far infrared (THz) optical constants of solids, liquids and gases to be determined from the amplitude and phase spectra of suitable samples measured at normal incidence in reflection or transmission experiments. DFTS was first developed in the 1960s by Chamberlain et al at the National Physical Laboratory in Teddington, UK [1, 2], and Bell et al in Columbus, Ohio [3,4]. The technique was later further developed by many others [5-10], and several reviews of the subject have been published [11-13].

The sample is placed in one arm of a Michelson interferometer, usually in one of the configurations shown in Fig. 1, and an asymmetric interferogram is recorded. For the reference measurement the interferometer is returned to a symmetric configuration by removing the sample and a second, symmetric, interferogram is recorded. The complex Fourier transforms of the two interferograms are computed and the amplitude and phase spectra of the sample are computed from the complex ratio of the two Fourier transforms. Finally, the optical constants or dielectric functions are calculated from the amplitude and phase spectra using the Fresnel relations. Details of the theory of DFTS have been given elsewhere [11].

DFTS has been found most useful when either the physical problem justifies its use, or when accurate values of the optical constants of a material are required for technical reasons. Two examples of the former are investigations of mode anharmonic self energies in simple ionic solids, and soft mode behaviour in ferroelectric crystals.

An example of an instrument designed for amplitude reflection spectroscopy of solids is shown in Fig. 2 [14]. This instrument has a number of novel features. (i) The far infrared radiation beams are focussed in both arms of the interferometer so that small samples can be studied. Focussing is achieved in each arm with an off-axis parabolic mirror and two plane mirrors, or, when the sample is present in the fixed arm, with an off-axis parabolic the case if only the small end mirror were scanned. (iv) The beam from a He-Ne laser is passed along the optic axis of the interferometer so that two interferograms are recorded simultaneously:

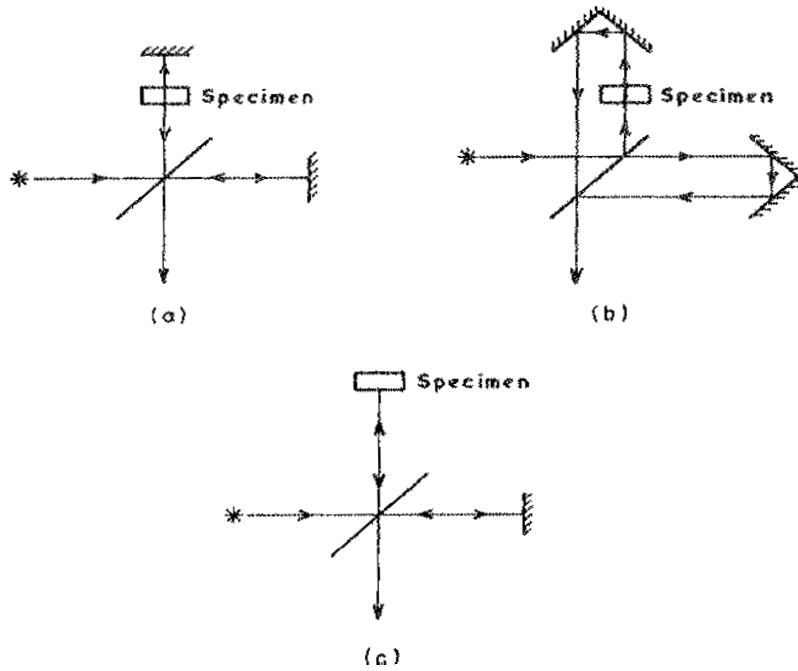


Fig. 1 The three main configurations for dispersive Fourier transform spectroscopy. (a) double-pass dispersive transmission spectroscopy, (b) single-pass dispersive transmission spectroscopy, and (c) dispersive, or amplitude, reflection spectroscopy.

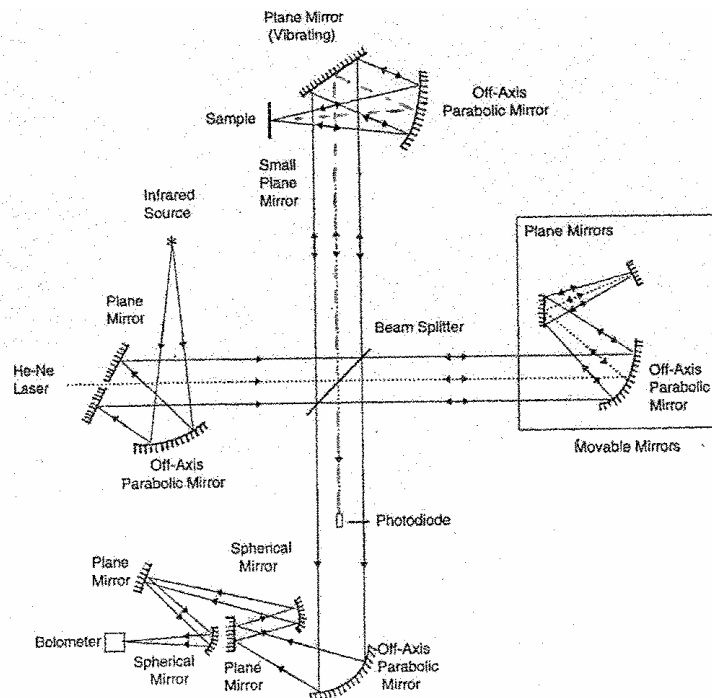


Fig. 2 Schematic drawing of a Michelson interferometer arranged for dispersive, or amplitude, reflection measurements on solids.

the conventional far infrared interferogram, and co-sinusoidal fringes from the modulation of the laser beam. (v) To obtain smooth mirror, one plane mirror and the sample. (ii) In the moving mirror arm the three mirrors are all bolted to a movable table so that when the table is scanned the three mirrors are scanned as a unit; this ensures that coherence is not lost when

the interferometer is scanned, as would be laser fringes the movable table is mounted on a high precision slide and scanned continuously [15]. The laser fringes are used to measure the optical path difference when the interferometer is scanned, but they also enable systematic phase errors to be eliminated, as discussed below. Continuous scanning of the interferometer produces a filtering envelope for the far infrared beam. Each spectral component is modulated at a different frequency which is determined by the scan speed, and the detector will only accept spectral components modulated at frequencies within its bandwidth. Thus, the scan speed can be set to tune the measured far infrared bandwidth to the detector bandwidth.

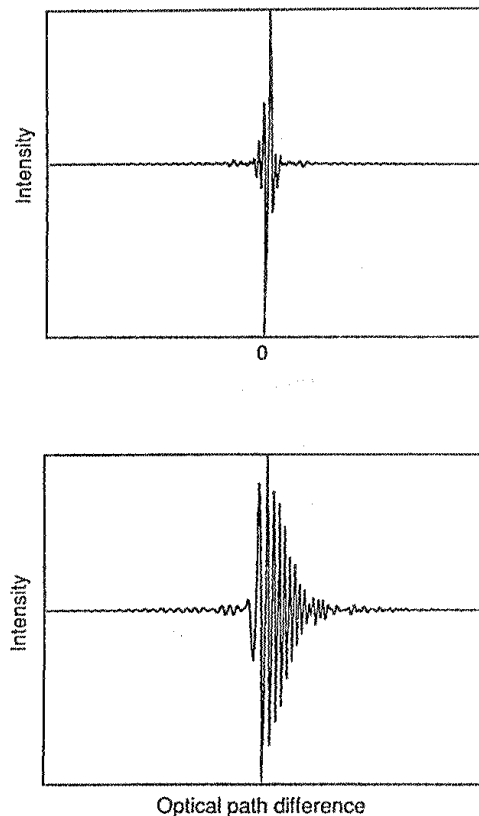


Fig. 3 Typical forms of background (top) and sample (bottom) interferograms obtained in reflection DFTS.

In reflection DFTS of solids it is necessary to record one interferogram using a reference mirror in the fixed arm and a second after replacing the reference mirror with the specimen. In early work great emphasis was placed on placing the reflecting surface of the specimen in “exactly” the same plane as the surface of the reference mirror to avoid systematic phase errors. The precision required in the physical replacement of these two surfaces is very high, corresponding to  $\sim 0.1 \mu\text{m}$  if the systematic phase error is to be reduced to below  $\sim 0.5^\circ$  at  $300 \text{ cm}^{-1}$  [11]. Unfortunately this is right at the limit of mechanical engineering, so enormous effort was required in the design of instruments to achieve this specification. Fortunately there is a much easier way of doing it. If a reference laser beam is transmitted along the optical axis of the instrument as shown in Fig. 2, the laser fringes can be used to monitor the optical path difference in the interferometer at the same time as compensating for systematic phase errors [16].

The precision with which the fringes can be sampled is determined by the signal to noise ratio,  $S/N$ , of the laser. With a simple, i.e. unstabilised, He-Ne laser with  $(S/N) \sim 100$ , the

equivalent positional uncertainty is  $\sim 6 \times 10^{-3} \mu\text{m}$ , which is good enough to reduce systematic phase errors to well below the level of random noise in far infrared work. Using a stabilised He-Ne laser, i.e.  $S/N \geq 1000$ , systematic positional errors can be reduced to the Ångstrom level, enabling DFTS measurements to be made at frequencies up to the ultraviolet [16]. Monitoring the optical path difference in this way automatically eliminates all systematic phase errors, including those due to drift in the lengths of the interferometer arms due to thermal expansion, backlash in micrometers, which is present in step-drive interferometers, and those due to inaccurate replacement of the reflecting surfaces of the sample and reference mirror. The laser beam also facilitates alignment of the interferometer. Further details are given elsewhere [16].

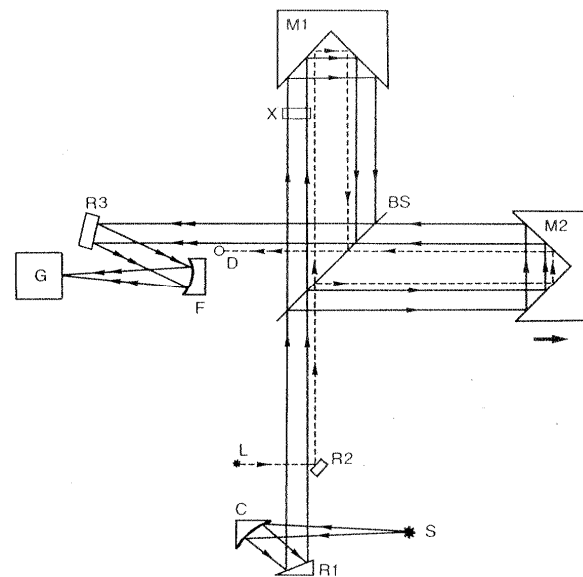


Fig. 4 Schematic drawing of an instrument designed for single-pass dispersive transmission measurements on solids.

In spectral ranges where the reflectivity is very low, which, in alkali halide crystals corresponds to everywhere except the reststrahl band, the phase is close to zero, so that both  $r$  and  $\phi$  are difficult to measure accurately by reflection DFTS. However, there is still important information in the spectrum close to the reststrahl band, and this can best be obtained by carrying out single-pass dispersive transmission measurements. Single pass measurements enable more accurate data to be obtained each side of the reststrahlen band than double-pass measurements, and an instrument designed for this purpose is shown in Fig. 4 [17]. The instrument is designed with two roof-top mirrors so that the outward and return beams in the two arms of the interferometer are physically offset. This enables a sample, X, to be placed in the fixed arm for single-pass transmission measurements. The instrument again has the beam from a He-Ne laser passing along the optic axis in both arms.

Typical forms for the background and sample interferograms are shown in Fig. 5. The first signature,  $I_0(x)$ , is the background interferogram. The second signature,  $I_s(x)$ , is the primary interferogram from the single pass of the infrared beam through the sample after the sample is inserted, and the third signature, at the far right, is from the first internal reflection of the infrared beam within the sample. Often, in measurements on transparent solids, only the signature  $I_s(x)$  from the sample need be included in the analysis.

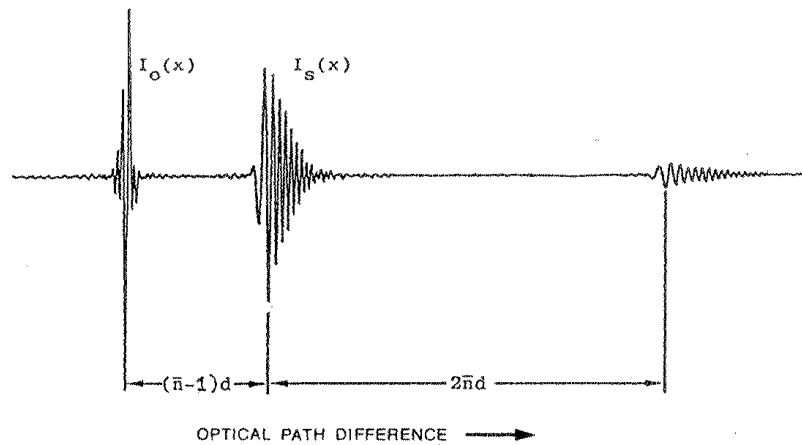


Fig. 5 Typical form of the interferograms obtained using single-pass dispersive transmission spectroscopy of solids.

## 2. DFTS Measurements

The determination of mode anharmonic self-energies in alkali halide crystals for comparison with calculations by quantum field theory requires an accurate knowledge of both optical constants in the region of the reststrahlen band, and this information is best obtained by DFTS. As an example of this, the amplitude and phase reflection spectra of KBr determined by reflection DFTS at 300 and 100 K [18] are shown in Fig. 6.

The optical constants or dielectric functions can be determined from the complex reflectivity using the Fresnel relations. The dielectric response of a simple ionic solid can be described approximately by a classical damped simple harmonic oscillator model in which a simple phenomenological damping constant is used which neglects the interactions between the normal modes. Maradudin and Fein [19] and Cowley [20] showed that the interactions between the normal modes can be taken into account using the methods of diagrammatic

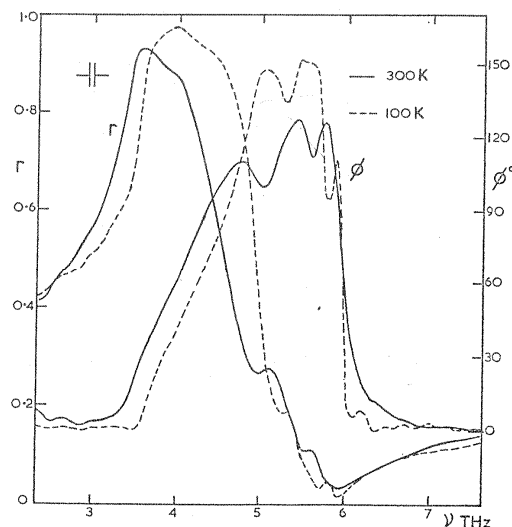


Fig. 6 The far infrared amplitude and phase reflection spectra of KBr measured at 300 and 100 K by reflection DFTS.  $3 \text{ THz} = 100 \text{ cm}^{-1}$ .

perturbation theory, leading to a complex frequency dependent damping coefficient for the zone centre transverse optic (TO) phonon mode. The imaginary part,  $\Gamma(\nu)$ , of this complex damping coefficient is shown in Fig. 7, where it is compared with calculations by Bruce [21]. The experimentally measured curve shown here has been determined from the amplitude reflection measurements of Fig. 6 between about 100 and 200  $\text{cm}^{-1}$ , and single pass dispersive transmission measurements (not shown here) either side.

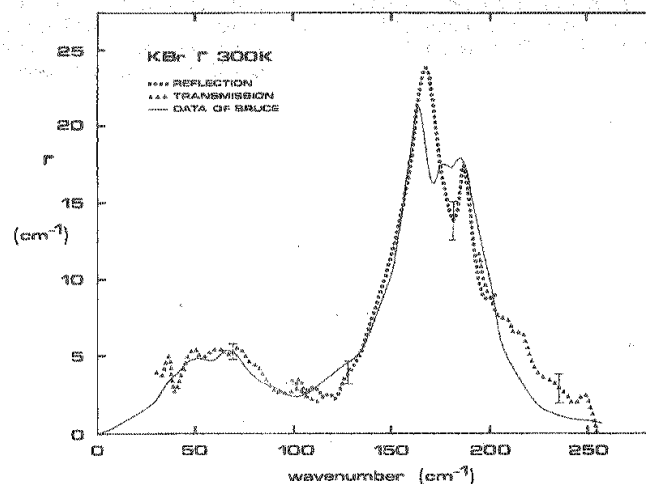


Fig. 7 A comparison of experimental and calculated results for the anharmonic self-energy,  $\Gamma(\nu)$ , of KBr at 300 K. Experimental results determined from  $(\epsilon', \epsilon'')$  obtained by reflection and transmission DFTS. Theoretical curve calculated by Bruce [21].

Another example where measurements by reflection DFTS are an advantage is soft mode behaviour in ferroelectrics. This behaviour occurs at low frequencies, and conventional measurements must be made over a wide frequency range, usually from the microwave region to the near IR, to determine the optical constants with sufficient accuracy using a Kramers-Kronig analysis. Using DFTS the information can be obtained in a single measurement, and the results of such measurements on  $\text{KTaO}_3$  at 100, 200 and 300 K are shown in Fig. 8 (top) [22]. In the lower part of the figure the conductivity,  $\sigma(\nu) = (\nu\epsilon''(\nu))/2$ , is plotted, where  $\nu$  is the wave number.

In ferroelectrics the static dielectric constant,  $\epsilon_0$ , follows the well-known form of Curie's law,  $\epsilon_0 \propto 1/(T-T_c)$ , above the ferroelectric transition temperature. It can be shown that this behaviour can be linked, via a generalised form of the Lyddane-Sachs-Teller relation [23], to the temperature dependence of the frequency,  $\omega_T$ , of the lowest frequency transverse optic, or "ferroelectric" mode, which is then expected to vary as  $\omega_T^2 \propto T$ .

The frequency of the lowest frequency peak of  $\sigma(\omega)$  in Fig. 8 (bottom) corresponds to  $\omega_T$ . Plotting  $\omega_T^2$  found in this way versus T gives the result shown in Fig. [9], and it can be seen that the results are in excellent agreement with the earlier results of Perry and McNelly [24] which were obtained by the much more laborious method of power reflection spectroscopy followed by a Kramers-Kronig analysis to obtain the phase.

DFTS has also been widely used to characterise semiconductors. An example of DFTS reflection measurements on a bulk single crystal of a III-V semiconductor is shown in Fig.10. The amplitude and phase reflection spectra,  $r$  and  $\phi-\pi$ , and the optical constants,  $n$  and  $k$ , of

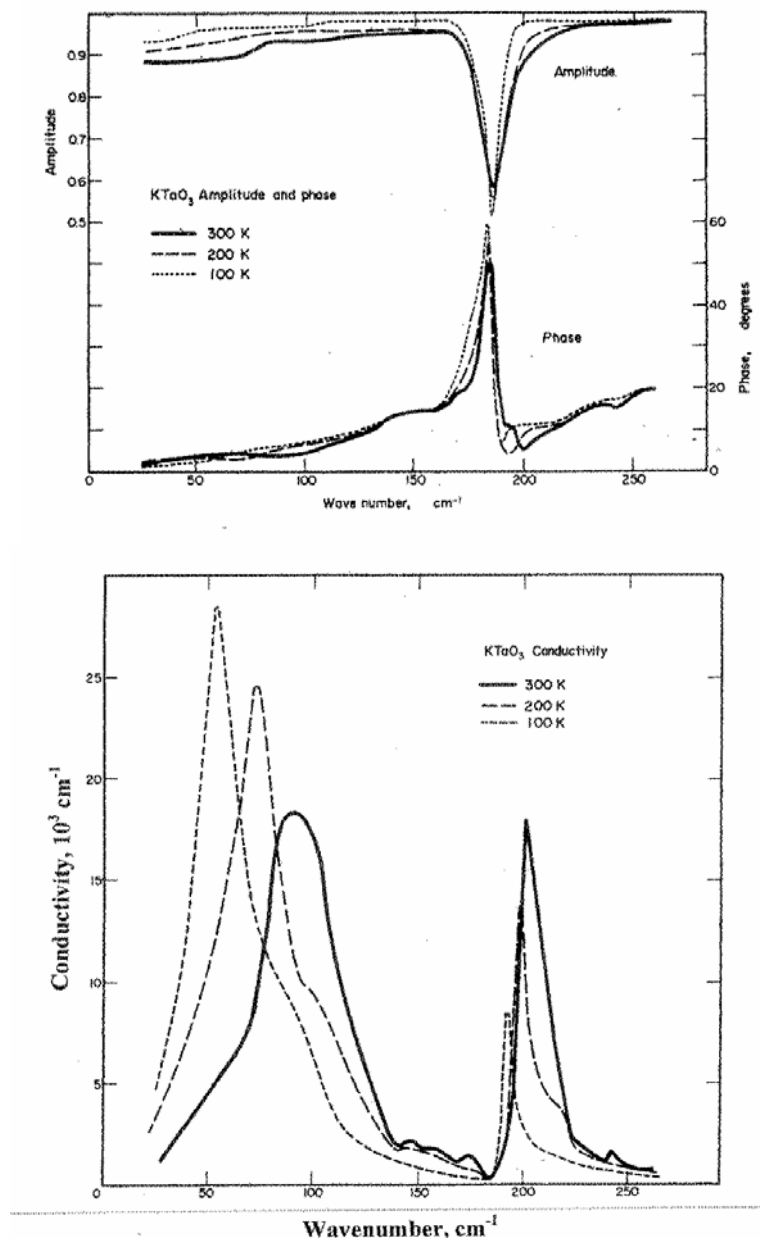


Fig. 8 The amplitude and phase of the far infrared reflectivity and the far infrared conductivity of KTaO<sub>3</sub> determined by reflection DFTS at 100, 200 and 300 K.

InSb measured at 300 K by reflection DFTS are shown here [25]. The phonon reststrahl band is clearly visible between 150 and 250  $cm^{-1}$  and the free carrier response below 150  $cm^{-1}$ . The phonon parameters and free carrier concentration were determined by fitting suitable response functions for the lattice response and bulk plasma response to this data. The phase reflection coefficient of samples lies between  $\pi$  and  $2\pi$  radians and the phase reflection coefficient of the reference mirror is  $\pi$  radians. Thus the measured phase difference is small, corresponding to a very small shift of the sample interferogram from the background interferogram, and this limits the accuracy of the determination of the refractive index in reflection DFTS to between about 1 and 5%. The accuracy of the determination of  $k$  is limited by the accuracy of the determination of  $\phi$ , as well as by the accuracy of the detector.

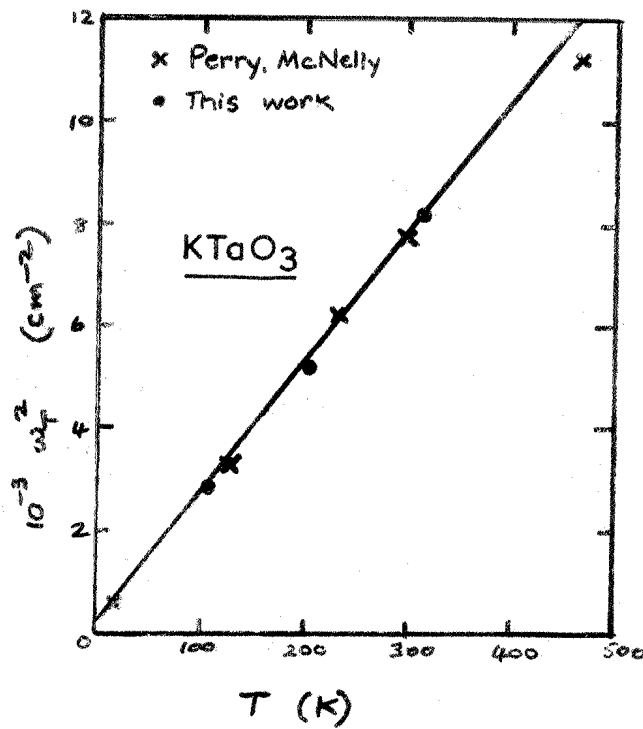


Fig. 9  $\omega_T^2$  plotted as a function of temperature for  $\text{KTaO}_3$ .

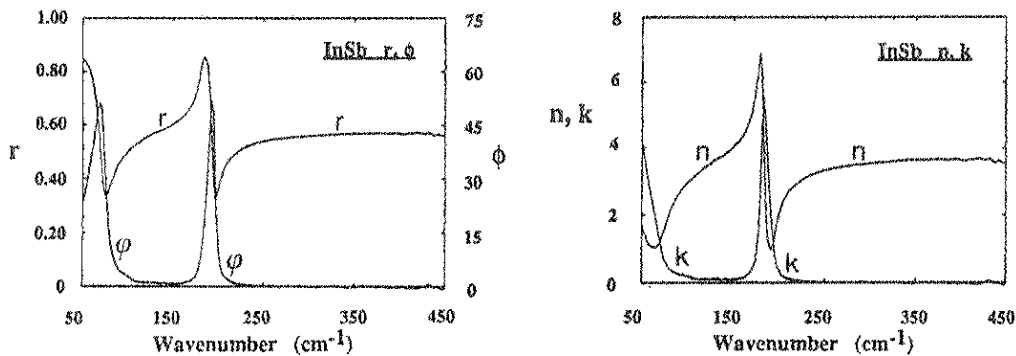


Fig.10 Left: the amplitude,  $r$ , and phase,  $\phi-\pi$ , reflection spectra of InSb measured at 300 K, and, Right: the calculated optical constants,  $n$  and  $k$ .

As in the case of alkali halide crystals, the optical constants of compound semiconductors cannot be measured accurately outside the reststrahlen and free carrier regions by amplitude reflection measurements, but this can be done by transmission DFTS. The optical constants of a single crystal of GaP of thickness 0.508 mm measured by single pass transmission DFTS at 300 K either side of the reststrahlen band, are shown in Fig. 11 [26, 27]. Note that the GaP sample is thick and the refractive index is large, between 1.9 and 2.4 in the measured range, so that the shift between the sample and background interferograms (not shown) for this sample would be large, similar to that shown in Fig. 5. Consequently this shift can be measured very accurately and it follows that in transmission DFTS of thick samples (several mm) the refractive index can be determined very accurately ( $\sim 1$  part in  $10^4$ ). The sample is opaque in the reststrahlen band between about 300 and 440  $\text{cm}^{-1}$ , and the structure either side arises from weak absorption due to phonon combination bands which can be assigned to specific transitions using a suitable lattice dynamical model [26, 27].

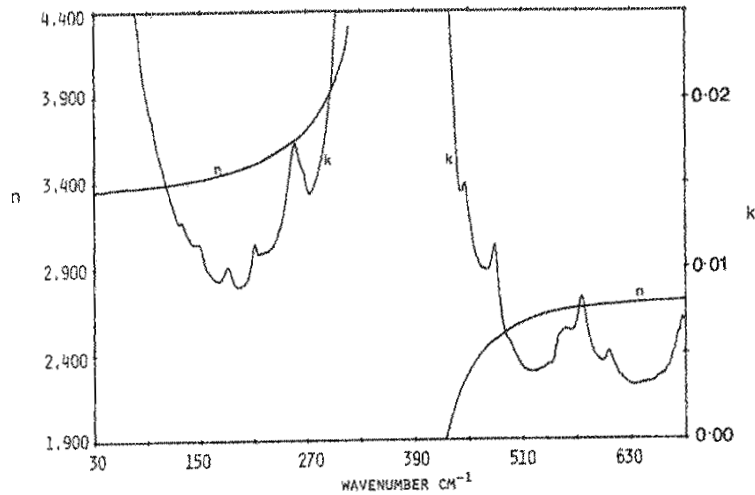


Fig. 11 The optical constants of a single crystal of GaP at 300 K either side of the reststrahl band determined by single-pass DFTS.

An example of work on a mixed II-VI semiconductor is shown in Fig. 12, where the extinction coefficient of a bulk mixed crystal of  $\text{Cd}_{0.22}\text{Hg}_{0.78}\text{Te}$  (CMT) determined by reflection DFTS is compared with a calculated spectrum [28]. The main features in the spectrum are the HgTe-like and CdTe-like reststrahl bands at 125 and 150  $\text{cm}^{-1}$  and the free carrier response below 80  $\text{cm}^{-1}$ , which can be used to determine the carrier concentration. The fine structure is attributed to a phonon combination band.

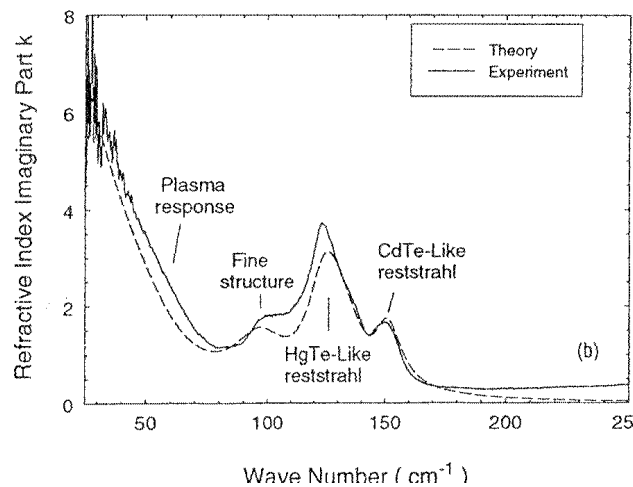


Fig. 12 The extinction coefficient,  $k$ , of a bulk mixed crystal of  $\text{Cd}_{0.22}\text{Hg}_{0.78}\text{Te}$  determined by reflection DFTS at 300 K.

### 3. Non-normal incidence methods

Although far infrared optical constants can be measured straightforwardly by DFTS, the technique is confined to measurements at normal incidence, so it cannot probe excitations in which the dielectric polarisation is not parallel to the sample surface. Consequently there are a number of interesting excitations, including surface and interface polaritons, for which other techniques are required.

Bulk modes cannot propagate at frequencies in the reststrahl band, the region between the zone centre transverse optic, TO, and longitudinal optic, LO, phonon frequencies in which the real part of the dielectric function is negative. However, surface and interface modes can propagate in this band. The fields associated with these modes are polarised normal to the interfaces and they decay rapidly away from the respective interfaces. In addition, they have advanced wave vectors, as illustrated in Fig. 13, which shows calculated surface polariton dispersion curves at the air/CMT interface for the bulk mixed crystal of  $\text{Cd}_{0.22}\text{Hg}_{0.78}\text{Te}$  (CMT) [28] discussed above. The dispersion curves for these modes lie to the right of the light line, so they cannot be probed in a conventional reflectivity experiment. A scan line is also drawn for an ATR measurement at  $20^\circ$  angle of incidence using a Si prism. Coupling in an ATR experiment occurs at the points where the four dispersion curves cross the scan line. The dispersion curves correspond to a surface plasmon at  $63.2 \text{ cm}^{-1}$ , and surface phonon modes at  $108.4$ ,  $139.7$  and  $156.5 \text{ cm}^{-1}$ . We shall return to these dispersion curves later.

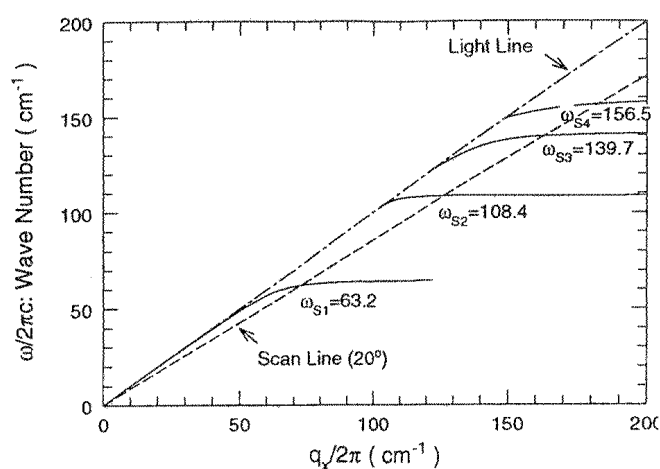


Fig. 13 Calculated surface polariton dispersion lines for a mixed crystal of  $\text{Cd}_{0.22}\text{Hg}_{0.78}\text{Te}$ . The drawing also shows the light line and an ATR scan line.

Two techniques for polarised oblique incidence reflection measurements are illustrated schematically in Fig. 14 below. A probe with a component of the electric vector normal to the sample surface is easily achieved by using p-polarised oblique incidence reflection spectroscopy (Fig. 14 (left) and Fig. 15 (centre)). s-polarisation measurements (Fig. 15 (left)) can be made by rotating the polariser through  $90^\circ$ . Wave vector enhancement for the investigation of non-radiative modes can be achieved by using either a grating or a prism [29, 30]. Using a grating at the sample surface the wave vector is enhanced by  $2n\pi/d$ , where  $n$  is an integer and  $d$  is the period of the grating. Using a prism (Fig. 14 (right) and Fig. 16), the radiation beam is incident internally on the base of the prism at an angle exceeding the critical angle for total internal reflection. This sets up an evanescent wave in the gap between the prism base and the sample with an enhanced in-plane wave vector component  $q_x = (\omega/c)\sin\theta\sqrt{\epsilon_p}$ , where  $\epsilon_p$  is the refractive index of the prism,  $\omega$  is the angular frequency and  $\theta$  is the angle of incidence. If the sample is placed close enough to the prism base the fields of the evanescent wave and the surface excitation overlap and the surface or interface mode is excited, causing a dip in the reflectivity at the mode frequency as shown in Fig. 16(c). However, care must be taken in the choice of an appropriate prism material.

Since the optical path length through the prism is long ( $\sim 2 \text{ cm}$  in this work), it is very important for the prism to be transparent, otherwise the beam will be seriously attenuated.

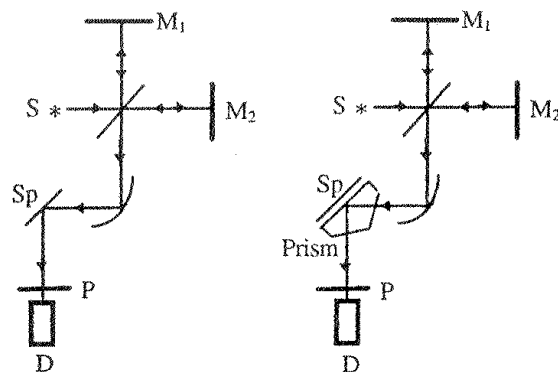


Fig.14 Schematic drawing of the experimental configuration for polarised reflection measurements (left) and polarised ATR measurements (right). S: radiation source, B: beam splitter, M<sub>1</sub> and M<sub>2</sub>, interferometer mirrors, Sp: sample, P: polariser, D: detector.  $d$  is the grating period and  $n$  is an integer.

Also, there should be as little dispersion as possible throughout the measured frequency range, or there will be significant curvature of the scan line. For work in the far infrared ( $\nu \sim 10\text{-}500\text{ cm}^{-1}$ ), the choice of prism material is limited to the elemental semiconductors (Si and Ge) and a few polymers. Polymers in general have very low refractive indices, but Si and Ge have high refractive indices, and dispersion is very low ( $\sim 1$  part in  $10^4$ ) in the far infrared because of the lack of first order phonon absorption. In this work single crystal Si, with  $n$  close to 3.143 throughout the measured frequency range has been used.

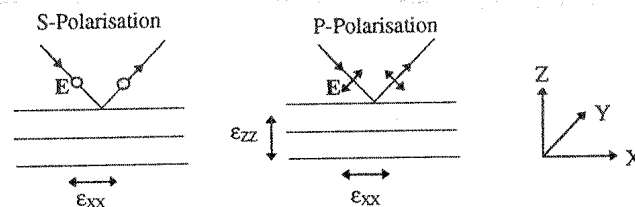


Fig.15 The two polarisation configurations and the coordinate axes. (Left) s-polarisation with the E vector normal to the plane of incidence, which couples only to  $\epsilon_{xx}$ , and (Centre) p-polarisation, with the E vector in the plane of incidence, which couples to both  $\epsilon_{xx}$  and  $\epsilon_{zz}$ .

A novel ATR stage developed for this work is illustrated schematically in Fig. 16(b). The prism and sample are mounted in a hole in a copper block (not shown in its entirety), and a micrometer screw is used to set the gap between the prism and the sample. For optimum coupling in dipole active samples such as simple ionic solids and binary semiconductors it is found that the gap width should be comparable with the free space wavelength at the excitation frequency. Thin ( $\sim 10\ \mu\text{m}$ ), narrow strips of copper foil are used as spacers to set the gap between the prism and the sample roughly, and the gap width is set precisely using the micrometer. The ATR stage is bolted to the base of a liquid nitrogen cold finger and placed in the output beam of the interferometer with the base of the prism at a focus. The range of external angles of incidence for the beam incident on the prism is about  $10^\circ$ , and this is reduced to about  $3^\circ$  inside the prism, so the polariton dispersion curves are sampled over a relatively narrow band of wave vectors, and this is not sufficiently large to affect the resolution significantly.

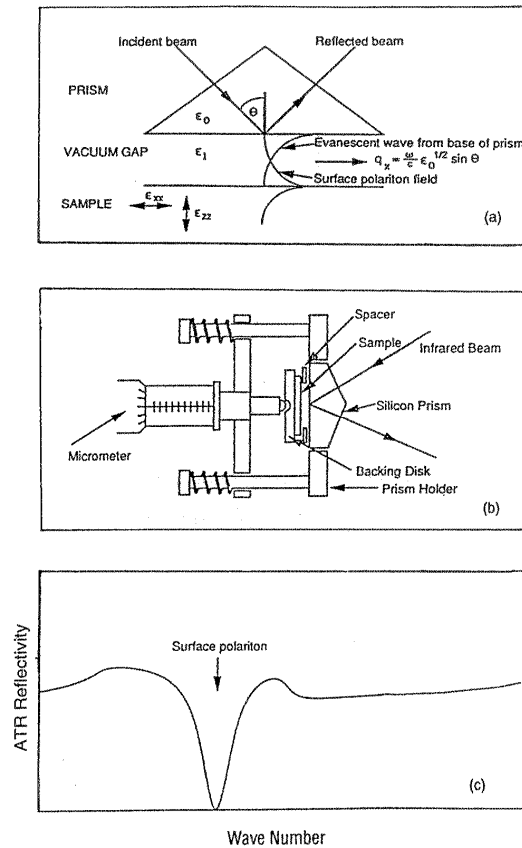


Fig. 16 (a) Schematic drawing of the incident and reflected radiation beams, evanescent wave and surface polariton field in an ATR experiment. (b) Details of the experimental ATR stage. (c) Appearance of the ATR dip observed in a measured spectrum.

#### 4. Non-normal incidence measurements

Semiconductor superlattices are fabricated for a variety of electronic and optical applications, and the quality of the interfaces is important as interface roughness causes a great deal of electron scattering. Some structures are fabricated from alternate materials such as GaAs and AlAs, in which there is no overlap between the frequencies of the optical branches of the phonon dispersion curves, so that optical phonons excited in one component cannot propagate across the bounding interfaces to the neighbouring component, and vice versa. Thus the optical phonons are confined in their respective layers and behave like standing waves with frequencies determined by the thicknesses of the layers and the bulk optical phonon dispersive curves. If the superlattice structure is of poor quality and the interfaces are broad due to alloying, there will be a change in the effective width of the layers. This leads to small shifts in the frequencies of the confined phonons which can be measured and used to obtain a quantitative estimate of the amount of interface broadening. An example of measured features in reflection spectra due to confined TO and LO phonons in GaAs/AlAs superlattices is shown in Fig. 17 [31]. These results were obtained by polarised oblique incidence reflection spectroscopy. From an analysis of the data it was found that the amount of interface broadening was  $\sim 1.4$  atomic spacings, in agreement with estimates from other techniques.

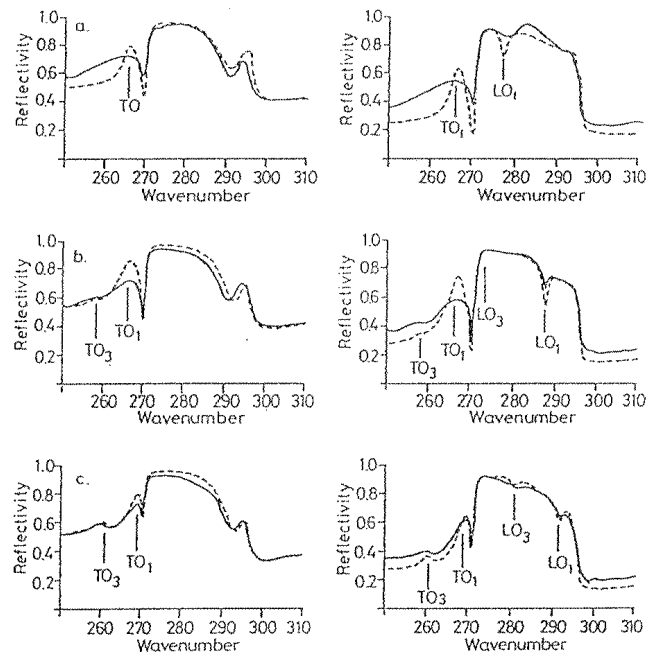


Fig. 17 Measured (solid lines) and calculated (dashed lines) oblique incidence ( $45^\circ$ ) reflectivity spectra at 77 K of three short period  $(\text{GaAs})_n(\text{AlAs})_n$  superlattices on GaAs substrates:  $n$  denotes the number of monolayers. (a)  $n = 2$ , (b)  $n = 4$ , (c)  $n = 6$ . Left hand curves: s-polarisation, right hand curves: p-polarisation. Note that the strong reststrahl reflectivity is from the GaAs substrates and the fine structure is due to the confined modes. The subscripts 1, 2, 3 denote the orders of the confined modes.

An example of a p-polarised ATR spectrum is shown in Fig.18 [14, 28], which should be compared with the extinction coefficient measured for the same sample by DFTS (Fig. 12), as those results indicate the frequency ranges occupied by the phonon reststrahl regions and the plasmon response, i.e., the regions in which surface and interface modes can propagate because the real part of the dielectric function is negative. Calculated surface polariton dispersion curves for this sample are shown in (Fig. 13). The advanced wave vector in the ATR experiment couples with the surface plasmon polariton at  $63.2 \text{ cm}^{-1}$  and the surface phonon polaritons in the CMT mixed crystal revealing the HgTe-like surface phonon polariton at  $139.7 \text{ cm}^{-1}$  and the CdTe-like polariton at  $156.5 \text{ cm}^{-1}$ . The calculated surface phonon polariton at  $108.4 \text{ cm}^{-1}$  is barely observable.

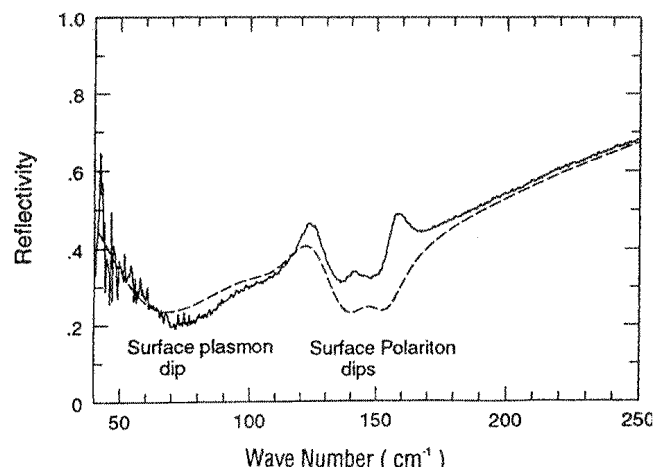


Fig. 18 Measured (continuous line) and calculated (dashed line) ATR spectrum of a bulk mixed crystal of  $\text{Cd}_{0.22}\text{Hg}_{0.78}\text{Te}$  at 300 K.

## 5. Summary

A number of far infrared techniques, including DFTS, polarised oblique incidence reflection spectroscopy and polarised attenuated total reflection (ATR) spectroscopy have been reviewed briefly, and the application of these techniques to the study and characterisation of a variety of solids, including alkali halide crystals, pseudo-displacive ferroelectrics and bulk and low dimensional semiconductors has been discussed.

## Acknowledgement

I am greatly indebted to Professor D H Martin of Queen Mary College, University of London, who first introduced me to the topic of far infrared spectroscopy of solids many years ago, and to all of my co-authors in the publications cited below, without whom this work would not have been possible.

## References

- [1] J. E. Chamberlain, J. E. Gibbs and H. A. Gebbie, *Nature (London)*, 198, 874-875, (1963).
- [2] J. E. Chamberlain, F. D. Findlay and H. A. Gebbie, *Nature (London)*, 206, 886-887, (1965).
- [3] E. E. Bell, *Jpn. J. Appl. Phys. (Suppl. I)* 4, 412-416, (1965).
- [4] E. E. Bell, *Infrared Phys.*, 6, 57-74, (1966).
- [5] J. Gast and L Genzel, *Opt. Commun.*, 8, 26-30, (1973).
- [6] T. J. Parker, W. G. Chambers and J. F. Angress, *Infrared Phys.*, 14, 207-215, (1974).
- [7] D. D. Honijk, W. F. Passchier and M. Mandel, *Physica*, 59, 536-540, (1972).
- [8] P. R. Staal and J. E. Eldridge, *Infrared Phys.*, 17, 299-303, (1977).
- [9] J. R. Birch, *Infrared Phys.*, 18, 275-282, (1978).
- [10] M. N. Afsar and J. B. Hasted, *J. Opt. Soc. Am.*, 67, 902-904, (1977).
- [11] J. R. Birch and T. J. Parker, *Dispersive Fourier transform spectroscopy*, Ch. 2 in *Infrared and Millimeter Waves*, Ed. K. J. Button, Academic Press, New York, (1979).
- [12] J. R. Birch, *Mikrochim. Acta (Wien)*, vol. III, 105-122, (1987).
- [13] T. J. Parker, *Contemporary Phys.*, 31, 335-353, (1990).
- [14] S. Farjami Shayesteh, Ph.D. Thesis, University of Essex, UK, (1996).
- [15] N. J. Burton and T. J. Parker, *Int. J. Infrared and Mm. Waves*, 5, 803-814, (1984).

- [16] N. J. Burton and T. J. Parker, *J. Modern Optics*, 36, 1103, (1989).
- [17] A. K. Wan Abdullah and T. J. Parker, *Infrared Phys.*, 29, 799-803, (1989).
- [18] T. J. Parker and W. G. Chambers, *IEEE Conf. Pub. No. 129*, 169, (1975).
- [19] A. A. Maradudin and A. E. Fein, *Phys. Rev.* 128, 2589, (1962).
- [20] R. A. Cowley, *Adv. Phys.*, 12, 421, (1963).
- [21] A. D. Bruce, *J. Phys. C6*, 174, (1973).
- [22] K. F. Pai, T. J. Parker, N. E. Tornberg and R. P. Lowndes, *Infrared Phys.*, 18, 327-336, (1978).
- [23] R. H. Lyddane, R. G. Sachs and E. Teller, *Phys. Rev.*, 59, 673, (1941).
- [24] C. H. Perry and T. F. McNelly, *Phys. Rev.*, 154, 456, (1967).
- [25] K. A. Maslin, C. Patel and T. J. Parker, *Infrared Phys.*, 32, 303-310, (1991).
- [26] A. K. Wan Abdullah, PhD Thesis, University of London, (1986).
- [27] A. K. Wan Abdullah, G. A. Gledhill, C. Patel and T. J. Parker, *Infrared Phys.*, 29, 719-723, (1989).
- [28] S. Farjami Shayesteh, T. Dumelow, T. J. Parker, T. I. Benushis, S. N. Ershov and M. I. Vasilevskiy, *Int. J. Infrared and Mm. Waves*, 16, 763, (1995).
- [29] A. Otto, in *Optical Properties of Solids: New Developments*, Ed. B. U. Seraphim, North-Holland, Amsterdam, p. 678, (1976).
- [30] V. V. Bryksin, Y. M. Gerbshtein and D. N. Mirlin, *Sov. Phys. Sol. State*, 13, 1779, (1971).
- [31] T. Dumelow, A. A. Hamilton, T. J. Parker, D. R. Tilley, C. T. Foxon, D. Hilton and K. J. Moore, *Int. J. Infrared and Mm. Waves*, 11, 901, (1990).